Optimal Candlestick-Based Spot Volatility Estimation: New Tricks and Feasible Inference Procedures*

Tim Bollerslev† Jia Li‡ Qiyuan Li§ Yifan Li¶

November 4, 2025

Abstract

We contribute to the growing literature on high-frequency spot volatility estimation by deriving a new integral representation for the recently introduced Asymptotic Minimum Risk Equivariant (AMRE) candlestick-based class of estimators. Our new theoretical representation enables the practical numerical computation of the hitherto impractical to compute optimal estimators based on multiple adjacent candlesticks. We also propose a new exact sampling scheme for high-frequency candlestick data, which facilitates straightforward calculation of the asymptotic risk and confidence intervals for the estimators. The resulting critical values for the highest-density intervals highlight the substantial efficiency gains from incorporating more than one candlestick in the estimation process. We showcase the practical value of the new techniques in elucidating the behavior of financial market volatility around the time of important news announcements.

Keywords: spot volatility, nonparametric estimation, range-based estimation, high-frequency candlestick data, numerical methods.

JEL Codes: C14, C22.

*We would like to thank Roberto Renò (discussant) and participants at 2025 SETA, Annual Meeting of SoFiE in Paris, and various seminars for useful comments on the new material presented in the paper as well as closely related work that inspired the paper. Jia Li's research is partially supported by a Singapore Ministry of Education tier-1 grant (22-SOE-SMU-016). MATLAB code for the practical implementation of the new numerical methods proposed in the paper are provided in an online supplement.

†Department of Economics, Duke University, Durham, NC 27708, and NBER; e-mail: boller@duke.edu.

‡School of Economics, Singapore Management University; e-mail: jiali@smu.edu.sg.

§Corresponding author. Faculty of Business and Economics, University of Hong Kong; e-mail: qiyuanli@hku.hk.

¶Accounting & Finance Division, University of Manchester; e-mail: yifan.li@manchester.ac.uk.

1 Introduction

Volatility plays a crucial role in asset pricing, portfolio and risk management, and the pricing and trading of derivative financial instruments. Volatility, and the estimation thereof, also sits at the core of financial econometrics. Some of the earliest formal estimators of volatility, dating back almost half-a-century, relied on parametric methods together with the high-low price range observed over a fixed time interval, typically a day or longer (Parkinson (1980) and Garman and Klass (1980)). Meanwhile, starting in the mid to late eighties, the focus of the volatility literature largely shifted to the use of parametric (G)ARCH and stochastic volatility type models (see, e.g., the surveys by Bollerslev et al. (1994) and Ghysels et al. (1996)). This was subsequently followed by another shift almost two decades later to the predominant use of nonparametric so-called realized volatility measures (Andersen and Bollerslev (1998) and Barndorff-Nielsen and Shephard (2002), as surveyed in Andersen et al. (2006)). More recently, motivated by the speed of today's financial markets and the popular use of identification schemes predicated on economic news announcement effects, there has been an increased focus on the estimation of volatility over ever finer intraday time intervals, with the resulting estimators often interpreted as proxies for the latent instantaneous, or spot, volatility at a given point in time (see, e.g., the recent studies by Li and Linton (2023) and Figueroa-López and Wu (2024), along with the introductory discussion in Andersen and Bollerslev (2018)).[1]

This more recent literature on spot volatility estimation typically relies on high-frequency intraday, or tick-by-tick level, price data. However, such data can be both costly and difficult to obtain, especially for many international markets and assets. By contrast, "candlestick data" comprised of the first (open) and last (close) prices together with the highest and lowest prices over short intraday time intervals, often down to one-minute, are now readily available for a host of different assets and markets through public databases (e.g., Yahoo Finance), commercial data services (e.g., Bloomberg), and various trading platforms (e.g., Robinhood). This has also spurred explorations into the use of such high-frequency mixed data for enhanced volatility estimation. Until fairly recently, however, these studies have generally relied on the direct use of the range-based estimators originally proposed for daily and lower frequency data almost half-a-century ago (e.g., Christensen and Podolskij (2007, 2012), Martens and van Dijk (2007), and Li et al. (2024)). Meanwhile, as shown by Bollerslev et al. (2024), the traditional range-based estimators are in general suboptimal in the high-frequency setting. They also do not fully exploit all the features and

[1] The option-implied SPOTVOL index for the S&P 500 (based on the methodology in Todorov (2019) and Todorov and Zhang (2022)) recently introduced by the CBOE as a complement to the ubiquitous one-month VIX index also underscores this renewed focus on spot volatility.

information embedded in the candlestick data. In an effort to rectify these deficiencies, Bollerslev et al. (2024) derived the class of optimal high-frequency candlestick-based spot volatility estimators, with the exact form of the optimal estimators explicitly geared to the relevant loss criteria.

Unfortunately, the semi-closed form expressions for the new optimal estimators derived in Bollerslev et al. (2024) are computationally challenging to implement in practice, and effectively infeasible when jointly considering the information in more than two candlesticks. As such, the numerical illustrations and efficiency comparisons presented in their paper are also limited to estimators based on only two candlesticks. This difficulty essentially arises from a curse-of-dimensionality problem associated with the computation of certain multivariate conditional expectation functions. Motivated by these difficulties, we make several theoretical contributions to enable the practical implementation and numerical analyses of the new optimal estimators.

First, by incorporating new analytical insights into the formal derivations, we obtain a novel integral representation for the optimal estimators. This alternative representation conveniently bypasses the curse-of-dimensionality problem that plagues the practical implementation of the original theoretical expressions alluded to above, in turn rendering the calculation of the estimators practically feasible for any number of candlesticks.

Second, we propose a new exact sampling scheme for the simulation of candlestick data. Compared to the conventional Euler discretization scheme traditionally used for the simulation of discretely sampled diffusion processes, our approach is orders of magnitude computationally more efficient.[2] Importantly, the new approach also avoids the well-known "inward" biases associated with simulating extreme observations, and Brownian functionals in particular. This new method in turn enables precise calculations of the asymptotic risks of the candlestick-based estimators and the construction of confidence intervals. It also holds the promise of additional broader applications in other econometrics and statistics problems involving extreme Brownian functionals.

Third, we present new extensive numerical analyses to further clarify the asymptotic performance of the optimal estimators. Our new results underscore the sizable efficiency gains afforded by the now computationally feasible optimal estimators based on multiple candlesticks compared to other commonly used estimators. We also demonstrate that multiple-candlestick estimators constructed by simply combining single-candlestick estimators in an ad hoc fashion may perform quite poorly.[3] Our new numerical analyses also directly link the performance of the optimal estimators

[2]Several other tailor made numerical and simulation methods explicitly motivated by the difficulties associated with the practical calculation of various volatility estimators have also previously been proposed in the literature (see, e.g., Bladt and Sørensen (2014) and Bladt et al. (2016)).

[3]The early work by Foster and Nelson (1996) on rolling regressions and sample variance estimation similarly emphasized the importance of unequal weighting when volatility is time-varying (see also the more recent study by

to various features of the candlesticks, thereby more clearly illuminating where the efficiency gains are coming from.

Fourth, we illustrate the practical usefulness of the new estimators in an empirical application pertaining to the behavior of aggregate stock market volatility around the time of the announcement of key inflation indicators. The new optimal high-frequency candlestick-based estimators generally point to a sharp immediate spike along with significantly higher volatility for up to thirty minutes after the news releases. By comparison, the crude volatility estimates obtained by summing the high-frequency squared returns over short time intervals that are sometimes used in the literature provide a much "noisier" picture, making it difficult to tell how the market volatility changed in response to the news announcements.

The remainder of the paper is structured as follows. Section 2 introduces our new theoretical results and corresponding procedures for efficiently calculating the optimal spot volatility estimators along with our new efficient procedures for simulating candlestick data. Section 3 presents numerical analyses pertaining to the asymptotic risks of the estimators along with comparisons to other suboptimal estimators previously used in the literature. Section 4 presents an empirical application involving market volatility at the time of inflation news announcements. Section 5 concludes. All the proofs are deferred to the Appendix.

2 Feasible Optimal Candlestick-Based Volatility Estimation

This section details our new representation and practically feasible methods for the construction of optimal candlestick-based volatility estimators. It also presents our new exact sampling scheme for candlestick data. We begin by briefly reviewing the theoretical framework and the form of the optimal estimators originally presented in Bollerslev et al. (2024).

2.1 Theoretical background and semi-closed form AMRE estimators

We assume that the log-price process P is an Itô semimartingale defined on a filtered probability space $\big(\Omega, \mathcal{F}, (\mathcal{F}_t)_{t\geq 0}, \mathbb{P}\big)$ expressed as:

$$P_t = P_0 + \int_0^t b_s ds + \int_0^t \sigma_s dW_s + J_t, \quad 0 \leq t \leq T, \tag{2.1}$$

where the drift b and the volatility σ are càdlàg adapted processes, W is a standard Brownian motion, and J is a pure jump process driven by a Poisson random measure.[4] Our focus is on the

Ghysels et al. (2023)).

[4]For ease of presentation, we deliberately exclude microstructure noise. Relatedly, most vendors build their candlesticks from trade prices as opposed to quotes. High/low trade prices could, of course, still be contaminated by

pth power transformation of spot volatility at some fixed time t, that is σ_t^p. Empirically relevant choices for p include $p = 1$ (spot volatility), $p = 2$ (spot variance), and $p = -1$ (spot precision).

We construct an estimator of σ_t^p using candlesticks over k consecutive time intervals of the form $I_n \equiv \bigcup_{i=1}^k I_n^{(i)}$, where the ith interval is $I_n^{(i)} \equiv [(i-1)\Delta_n, i\Delta_n]$, and $t \in I_n$. The candlestick observation for each interval comprises the opening, high, low, and closing prices over $I_n^{(i)}$. The information about within-interval price movements can be summarized using the following normalized returns:

$$r_i \equiv \frac{R_{i\Delta_n}^{(i)}}{\sqrt{\Delta_n}}, \qquad h_i \equiv \frac{\sup_{t \in I_n^{(i)}} R_t^{(i)}}{\sqrt{\Delta_n}}, \qquad l_i \equiv \frac{\inf_{t \in I_n^{(i)}} R_t^{(i)}}{\sqrt{\Delta_n}}, \tag{2.2}$$

where $R_t^{(i)} \equiv P_t - P_{(i-1)\Delta_n}$. Accordingly, the candlestick return features for k successive intervals may be succinctly expressed as $\mathbf{C}_k = (r_i, h_i, l_i)_{1 \le i \le k}$.

We rely on infill asymptotic analysis, assuming that the length of the sampling interval $\Delta_n \to 0$, corresponding to the use of high-frequency candlestick observations. Additionally, we treat k as fixed, emphasizing the small-sample nature of the spot estimation problem. An estimator of σ_t^p based on k candlestick observations thus takes the generic form $f(\mathbf{C}_k)$, for some measurable function $f : \mathbb{R}^{3k} \to \mathbb{R}_+$. Since volatility represents a scale parameter, we focus on scale-equivariant estimators that satisfy $f(\lambda \mathbf{x}) = \lambda^p f(\mathbf{x})$ for all $\lambda > 0$ and $\mathbf{x} \in \mathbb{R}^{3k}$.

Adapting a small-sample "coupling" argument, it is possible to show that, with k fixed and $\Delta_n \to 0$, the estimation error of a scale-equivariant estimator $\hat{\sigma}_t^p = f(\mathbf{C}_k)$ admits a nonstandard limit distribution. Specifically, let $(\widetilde{W}^{(i)})_{1 \le i \le k}$ denote k mutually independent standard Brownian motions and define $\tilde{\boldsymbol{\zeta}}_k \equiv (\tilde{\zeta}_{i,r}, \tilde{\zeta}_{i,h}, \tilde{\zeta}_{i,l})_{1 \le i \le k}$ where

$$\tilde{\zeta}_{i,r} \equiv \widetilde{W}_1^{(i)}, \qquad \tilde{\zeta}_{i,h} \equiv \sup_{t \in [0,1]} \widetilde{W}_t^{(i)}, \qquad \tilde{\zeta}_{i,l} \equiv \inf_{t \in [0,1]} \widetilde{W}_t^{(i)}. \tag{2.3}$$

It then follows that:

$$\frac{\hat{\sigma}_t^p}{\sigma_t^p} \xrightarrow{d} f(\tilde{\boldsymbol{\zeta}}_k). \tag{2.4}$$

Importantly, the limit variable, $f(\tilde{\boldsymbol{\zeta}}_k)$, is pivotal and does not depend on any nuisance parameters.

This asymptotic result in turn enables the calculation of the asymptotic estimation risk. When the loss function is scale-invariant, this estimation loss may be conveniently expressed as $L(\hat{\sigma}_t^p / \sigma_t^p)$ for some loss function $L(\cdot)$. For any continuous loss function $L(\cdot)$, the continuous mapping theorem further implies that $L(\hat{\sigma}_t^p / \sigma_t^p) \xrightarrow{d} L\big(f(\tilde{\boldsymbol{\zeta}}_k)\big)$. Accordingly, the asymptotic risk of $\hat{\sigma}_t^p = f(\mathbf{C}_k)$

bid-ask bounce effects. However, as discussed in more detail in Bollerslev et al. (2024), for highly liquid assets with "sufficiently coarsely" sampled candlesticks this distortion is arguably negligible. For less liquid assets, where this effect can be more severe, the bias in the local extrema could be formally characterized using the results in Bibinger et al. (2016).

is given by $R(f,L) \equiv \mathbb{E}\big[L\big(f(\tilde{\boldsymbol{\zeta}}_k)\big)\big]$. Since the distribution of $\tilde{\boldsymbol{\zeta}}_k$ is known, this asymptotic risk can in principle be computed for any estimator $f(\cdot)$ and loss function $L(\cdot)$. The optimal estimator, which minimizes the asymptotic risk, is referred to as the Asymptotic Minimum Risk Equivariant (AMRE) estimator. However, the highly nonstandard distribution of the random vector $\tilde{\boldsymbol{\zeta}}_k$ severely complicates the functional minimization problem and the formal derivation of the optimal estimator.

More concretely, consider the two commonly used loss functions, Stein and quadratic:

$$L_{\text{Stein}}(x) \equiv x - \log x - 1, \qquad L_{\text{Quad}}(x) \equiv (x-1)^2. \tag{2.5}$$

In addition to the absolute return $|r_i|$, further define $w_i \equiv h_i - l_i$, representing the candlestick range, and $a_i \equiv |h_i + l_i - r_i|$, measuring its asymmetry. The AMRE estimators under the two loss functions may then be formally expressed as:

$$\begin{aligned}
\hat{\sigma}^p_{\text{Stein}}(k) &= w_1^p \cdot \frac{1}{F_{k,p}\Big(\frac{|r_1|}{w_1}, \frac{a_1}{w_1}, \frac{w_2}{w_1}, \frac{|r_2|}{w_1}, \frac{a_2}{w_1}, \cdots, \frac{w_k}{w_1}, \frac{|r_k|}{w_1}, \frac{a_k}{w_1}\Big)}, \\
\hat{\sigma}^p_{\text{Quad}}(k) &= w_1^p \cdot \frac{F_{k,p}\Big(\frac{|r_1|}{w_1}, \frac{a_1}{w_1}, \frac{w_2}{w_1}, \frac{|r_2|}{w_1}, \frac{a_2}{w_1}, \cdots, \frac{w_k}{w_1}, \frac{|r_k|}{w_1}, \frac{a_k}{w_1}\Big)}{F_{k,2p}\Big(\frac{|r_1|}{w_1}, \frac{a_1}{w_1}, \frac{w_2}{w_1}, \frac{|r_2|}{w_1}, \frac{a_2}{w_1}, \cdots, \frac{w_k}{w_1}, \frac{|r_k|}{w_1}, \frac{a_k}{w_1}\Big)},
\end{aligned} \tag{2.6}$$

where the function $F_{k,q} : \mathbb{R}^{3k-1} \to \mathbb{R}$ for $q \in \{p, 2p\}$ is defined as the conditional expectation:

$$\begin{aligned}
&F_{k,q}\Big(\frac{|r_1|}{w_1}, \frac{a_1}{w_1}, \frac{w_2}{w_1}, \frac{|r_2|}{w_1}, \frac{a_2}{w_1}, \cdots, \frac{w_k}{w_1}, \frac{|r_k|}{w_1}, \frac{a_k}{w_1}\Big) \\
&\quad \equiv \mathbb{E}\bigg[\tilde{\zeta}^q_{1,w} \;\Big|\; \frac{\tilde{\zeta}_{i,w}}{\tilde{\zeta}_{1,w}} = \frac{w_i}{w_1}, \frac{|\tilde{\zeta}_{i,r}|}{\tilde{\zeta}_{1,w}} = \frac{|r_i|}{w_1}, \frac{\tilde{\zeta}_{i,a}}{\tilde{\zeta}_{1,w}} = \frac{a_i}{w_1}, \forall 1 \le i \le k\bigg],
\end{aligned} \tag{2.7}$$

where $\tilde{\zeta}_{i,w} \equiv \tilde{\zeta}_{i,h} - \tilde{\zeta}_{i,l}$ and $\tilde{\zeta}_{i,a} \equiv |\tilde{\zeta}_{i,h} + \tilde{\zeta}_{i,l} - \tilde{\zeta}_{i,r}|$. These semi-closed form solutions effectively reduce the functional risk minimization problem to the computation of the conditional expectations defined in (2.7). Utilizing this representation, Bollerslev et al. (2024) were able to derive closed-form solutions for the case of $k = 1$, albeit fairly complicated ones. However, for $k > 1$, no such solutions are currently available.

Instead, a brute force numerical approach based on the use of Monte Carlo simulations combined with flexible nonlinear fitting procedures could in principle be used to calculate the requisite conditional expectation function. That is also the approach adopted for $k = 2$ in Bollerslev et al. (2024). However, since the dimensionality of the conditioning vector grows as $3k - 1$, such an approach is practically infeasible for $k > 2$. Alternatively, as we show next, by delving deeper into the analytical structure of the problem, it becomes possible to bypass this curse-of-dimensionality issue by reformulating the requisite computation as a univariate numerical integration, thereby facilitating the calculation of the AMRE estimator for any value of k.

2.2 Practical numerical computation of AMRE estimators

Our new and more efficient computational method involves an alternative representation of the AMRE estimators. To formalize the said representation, let $\phi(x) \equiv (2\pi)^{-1/2}e^{-x^2/2}$ denote the standard normal density function, with its second derivative denoted by $\phi''(x) \equiv (x^2-1)\phi(x)$. Also define the function $M_{k,p}(\mathbf{C}_k)$ as:

$$M_{k,p}(\mathbf{C}_k) \equiv \int_0^\infty v^{3k+p-1} \prod_{i=1}^{k} \tilde{g}(v|r_i|, vw_i, va_i)dv, \tag{2.8}$$

where

$$\tilde{g}(r,w,a) \equiv \sum_{m=-\infty}^{\infty} \big(m^2\phi''(2mw+r) - m(m+1)\phi''((2m+1)w-a)\big). \tag{2.9}$$

The latter effectively represents a "kernel" for the conditional density function associated with the conditional expectation in equation (2.7). Using this notation, the following proposition obtains (the requirement that $k \geq (1-2p)/3$ is only needed when $p<0$ to ensure that the $M_{k,p}(\cdot)$ functions are well defined).

Proposition 1. *For any $k \geq (1-2p)/3 \vee 1$, the AMRE estimators described in equation (2.6) can be represented as:*

$$\hat{\sigma}^p_{\text{Stein}}(k) = \frac{M_{k,0}(\mathbf{C}_k)}{M_{k,p}(\mathbf{C}_k)}, \qquad \hat{\sigma}^p_{\text{Quad}}(k) = \frac{M_{k,p}(\mathbf{C}_k)}{M_{k,2p}(\mathbf{C}_k)}.$$

Proposition 1 simplifies the computation of the AMRE estimator to evaluating the $M_{k,p}(\cdot)$ functions in (2.8). Importantly, this only requires a one-dimensional numerical integration. Although the integrand still involves the calculation of an infinite sum, as defined in (2.9), the corresponding summand terms converge exponentially fast as $|m| \to \infty$ and $v \to \infty$. In practice, one may therefore truncate the sum and the integral limits at a "sufficiently large" value with negligible loss of numerical precision. Consequently, the univariate integral may easily be computed to machine precision using textbook numerical techniques.[5] In practice, we truncate the sum in (2.9) to $|m| < M$ and the integral in (2.8) by $\int_\varepsilon^\Lambda(\cdot)dv$ where $\min\{\Lambda, \varepsilon^{-1}, \varepsilon M\} \to \infty$. Then the total truncation error satisfies

$$\text{Error}(\varepsilon, \Lambda, M) = O\Big(e^{-\frac{\pi^2}{4\varepsilon^2}} + M\Lambda^{p+1}e^{-\frac{\varepsilon^2M^2}{4}} + \Lambda^{p+1}e^{-\frac{\Lambda^2}{2}}\Big) = o(1).$$

Compared to the "brute force" approach used in Bollerslev et al. (2024) for handling multiple candlesticks, which relies on a Deep Neural Network (DNN) for estimating the entire optimal estimation function, our new method is substantially more computationally efficient. In particular,

[5] MATLAB codes for computing the estimators and implementing the exact simulations discussed below are available in the online supplement.

by directly leveraging the analytical insights into the distributions of the candlestick features, we bypass the difficult "blind" simulation-based nonparametric estimation of a multivariate conditional expectation function. Also, rather than trying to estimate the entire function $f(\cdot)$, our approach only requires the evaluation of the estimator at the observed data point $f(\mathbf{C}_k)$. This in turn combines to allow for a much more computationally efficient and accurate approach.

We turn next to a discussion of our new sampling method designed to efficiently and accurately simulate the requisite candlestick features that serves as the foundation for the numerical calculations of asymptotic risks and confidence intervals.

2.3 An exact sampling scheme for candlestick data

Let $\tilde{\boldsymbol{\zeta}}_k \equiv (\tilde{\zeta}_r, \tilde{\zeta}_h, \tilde{\zeta}_l)$ denote the random vector previously defined in Section 2.1, where for ease of notation we omit the subscript i. The primary challenge in simulating $\tilde{\boldsymbol{\zeta}}_k$ arises from the fact that $\tilde{\zeta}_h$ and $\tilde{\zeta}_l$ are both extreme functionals. These functionals are typically simulated using a standard Euler discretization scheme, in which a discretized Brownian motion is drawn from a "fine" mesh over the unit time interval. The extreme values, $\tilde{\zeta}_h$ and $\tilde{\zeta}_l$, are then simply approximated by the maximum and minimum of the discretized simulated process. However, these simulated extremes are invariably "inward" biased compared to their theoretical values (see Proposition 3 in Asmussen et al. (1995)). This bias could, of course, be reduced through the use of a very fine mesh. But, that will also substantially increase the computational cost. The cost is further compounded when a large number of simulations is required, as is the case in the present setting involving numerical calculations of asymptotic risks and confidence intervals by Monte Carlo methods.[6]

The following proposition provides a convenient cost-effective solution for the simulation of extreme Brownian functionals more generally.

Proposition 2. *Let r denote a random draw from $\mathcal{N}(0,1)$. Draw u and v independently from the uniform distribution $\mathcal{U}[0,1]$ and set $h = \big(r + \sqrt{r^2 - 2\log(1-u)}\big)/2$. Given r and h, set l as the solution to $v = F(l; r, h)$ where*

$$F(l; r, h) = 1 - \sum_{m=-\infty}^{\infty} \left(m \frac{\phi'\big(r - 2m(h-l)\big)}{\phi'(2h-r)} - (m+1) \frac{\phi'\big(r - 2m(h-l) - 2h\big)}{\phi'(2h-r)} \right),$$

in which $l \leq (r \wedge 0)$ and $\phi'(x) = -x\phi(x)$. It holds that $(r, h, l) \overset{d}{=} (\tilde{\zeta}_r, \tilde{\zeta}_h, \tilde{\zeta}_l)$.

To the best of our knowledge, the proposed algorithm for jointly simulating the terminal value, supremum, and infimum of a Brownian motion is novel. The method draws sequentially from

[6] For example, Li et al. (2024) conducts $N = 10^8$ simulations with $M = 10^7$ mesh points in a similar context, resulting in an extremely computationally expensive 10^{15} number of random draws.

the relevant conditional distributions, ensuring exact simulation from the target joint distribution. The only nontrivial computational step involves numerically solving the nonlinear equation $v = F(l; r, h)$, which entails an infinite sum. However, the monotonicity of $F(l; r, h)$ guarantees a unique solution and since the summands decay rapidly as $m \to \infty$, standard numerical methods can easily be used to accurately evaluate the sum to machine precision.

To more formally quantify the corresponding computational gains, note that the tailed sum of $F(l; r, h)$ over $|m| > K$ obeys an exponential bound of $\exp\{-2K^2(h-l)^2\}$. Hence, to achieve truncation error ε it suffices to take $K \asymp \sqrt{\log(1/\varepsilon)}$. Since $F(l; r, h)$ is strictly increasing, a one-dimensional inversion by iteration (e.g., Newton's method) requires $O\big(\log(1/\varepsilon)\big)$ function evaluations (see Theorem 5.2.3 in Stoer and Bulirsch (2002)). The per-draw cost of the proposed simulation scheme is therefore only $O\big(\log(1/\varepsilon)^{3/2}\big)$; i.e., polylogarithmic in the tolerance. By comparison, a conventional Euler scheme would require $O(\varepsilon^{-1/2})$ time steps per path to control the "inward" bias at level ε. Simply put, our new exact simulation scheme is not only bias-free, it is also highly computationally efficient.

3 Properties of Optimal Candlestick-Based Volatility Estimators

The new representation for the AMRE candlestick-based estimators in Proposition 1 and the exact sampling scheme for candlestick data in Proposition 2 combine to allow for the practical implementation and deeper numerical analysis of the theoretical properties of the optimal estimators. We begin our analyses by calculating the confidence intervals and the asymptotic risks of the estimators. We then compare the estimation risk of the optimal estimators to that of other suboptimal estimators previously proposed in the literature, further clarifying where the efficiency gains are coming from.

3.1 Confidence intervals and asymptotic risk

Our calculation of the confidence intervals relies on the same fixed-k inference approach used by Bollerslev et al. (2021, 2024). In particular, by simulating a large Monte Carlo sample for $\tilde{\boldsymbol{\zeta}}_k$, it is possible to numerically select an interval $[L_\alpha, U_\alpha]$ that satisfies the condition:

$$\mathbb{P}(L_\alpha \leq 1/f(\tilde{\boldsymbol{\zeta}}_k) \leq U_\alpha) = 1 - \alpha, \tag{3.10}$$

for a chosen confidence level $1 - \alpha$. Using the continuous mapping theorem together with (2.4), it follows that $\mathbb{P}(\sigma_t^p \in [L_\alpha \hat{\sigma}_t^p, U_\alpha \hat{\sigma}_t^p]) \to 1 - \alpha$, confirming that the interval $[L_\alpha \hat{\sigma}_t^p, U_\alpha \hat{\sigma}_t^p]$ achieves the correct asymptotic coverage. While there are infinitely many choices for $[L_\alpha, U_\alpha]$ that satisfy

this coverage criterion, it is natural to select the highest density (HD) interval, $[L_\alpha^{HD}, U_\alpha^{HD}]$, which minimizes the interval length $U_\alpha - L_\alpha$.

Table 1 provides the resulting critical values for various numbers of candlesticks, or block sizes $k \in \{1, \ldots, 20\}$, and the two standard confidence levels, 90% and 95%, for the spot volatility, σ_t, and the spot variance, σ_t^2, reported in Panels A and B, respectively. The optimal estimators under Stein's and quadratic loss functions are reported in the left and the right portions of the table, respectively. All of the calculations are based on one million Monte Carlo trials.

Comparing the results across rows, the length of the HD confidence intervals naturally narrows as the number of candlesticks k used in the estimation increases, underscoring the substantial efficiency gains afforded by the use of multiple adjacent candlesticks ($k > 1$) as opposed to a single candlestick ($k = 1$) in the estimation process. The intervals that obtain under quadratic loss are typically slightly wider than those under Stein's loss. The intervals are obviously also positioned differently under Stein's and quadratic loss, with the latter generally shifted slightly to the right, reflecting the relatively higher penalty associated with overestimation under quadratic loss.

Turning next to the risks of the estimators, for each estimation function $f(\cdot)$, we compute its asymptotic risk $\mathbb{E}\big[L\big(f(\tilde{\boldsymbol{\zeta}}_k)\big)\big]$ using Monte Carlo integration and the new exact sampling scheme for drawing $\tilde{\boldsymbol{\zeta}}_k$. To underscore that the AMRE estimators explicitly depend on the choice of loss function, we report their asymptotic risks under both Stein's and quadratic loss. In addition, we also compute the asymptotic bias and asymptotic variance of the estimators, defined in relative terms as:

$$\text{Bias} \equiv \mathbb{E}[f(\tilde{\boldsymbol{\zeta}}_k)] - 1, \qquad \text{Var} \equiv \mathit{Var}\big(f(\tilde{\boldsymbol{\zeta}}_k)\big). \tag{3.11}$$

Looking at the results summarized in Table 2, the biases of $\hat{\sigma}_{\text{Stein}}(k)$ and $\hat{\sigma}^2_{\text{Stein}}(k)$ are virtually zero for all values of k, consistent with the fact that the AMRE estimator under Stein's loss is unbiased (Brown, 1968).[7] By contrast, the biases for both $\hat{\sigma}_{\text{Quad}}(k)$ and $\hat{\sigma}^2_{\text{Quad}}(k)$ are systematically negative. This "shrinkage" naturally arises as a consequence of quadratic loss penalizing overestimation more severely than underestimation. The table also reveals that as k increases, the biases, variances, and risks of all the AMRE estimators decrease at an approximate rate of k^{-1}.

Consistent with the unique optimality of the AMRE estimators, the risk of $\hat{\sigma}^p_{\text{Stein}}(k)$ is obviously lower than that of $\hat{\sigma}^p_{\text{Quad}}(k)$ under Stein's loss, while the opposite holds true for the quadratic loss. Meanwhile, for larger values of k, say $k \geq 15$, the two AMRE estimators apparently enjoy very similar risks under both loss functions. This aligns with the common large-sample intuition that

[7] For $k = 1$, the numbers in Table 2 perfectly align with those in Bollerslev et al.'s (2024). For $k = 2$, however, slight discrepancies arise due to biases in the Euler discretization scheme and errors in estimating the functional relationships underlying the approximate numbers reported in Bollerslev et al.'s (2024).

Table 1: Critical Values for Highest Density Intervals of AMRE Estimators

Panel A: Estimators for Spot Volatility σ_t

$\hat{\sigma}_{\text{Stein}}(k)$					$\hat{\sigma}_{\text{Quad}}(k)$				
k	$L_{10\%}$	$U_{10\%}$	$L_{5\%}$	$U_{5\%}$	k	$L_{10\%}$	$U_{10\%}$	$L_{5\%}$	$U_{5\%}$
1	0.6354	1.4793	0.5950	1.6088	1	0.6744	1.5715	0.6361	1.7159
2	0.7350	1.3182	0.6964	1.3950	2	0.7568	1.3582	0.7189	1.4397
3	0.7796	1.2515	0.7482	1.3122	3	0.7950	1.2765	0.7650	1.3409
4	0.8103	1.2173	0.7787	1.2648	4	0.8232	1.2364	0.7920	1.2856
5	0.8288	1.1914	0.8014	1.2344	5	0.8388	1.2058	0.8116	1.2499
10	0.8788	1.1332	0.8565	1.1603	10	0.8848	1.1407	0.8624	1.1680
15	0.9003	1.1077	0.8826	1.1300	15	0.9041	1.1123	0.8864	1.1347
20	0.9126	1.0919	0.8984	1.1121	20	0.9153	1.0952	0.9010	1.1154

Panel B: Estimators for Spot Variance σ_t^2

$\hat{\sigma}^2_{\text{Stein}}(k)$					$\hat{\sigma}^2_{\text{Quad}}(k)$				
k	$L_{10\%}$	$U_{10\%}$	$L_{5\%}$	$U_{5\%}$	k	$L_{10\%}$	$U_{10\%}$	$L_{5\%}$	$U_{5\%}$
1	0.3671	2.2246	0.3186	2.6529	1	0.4583	2.8071	0.4019	3.3659
2	0.5123	1.7317	0.4624	1.9523	2	0.5784	1.9544	0.5181	2.2027
3	0.5891	1.5601	0.5357	1.7116	3	0.6371	1.6898	0.5804	1.8565
4	0.6435	1.4751	0.5930	1.5955	4	0.6764	1.5596	0.6267	1.6924
5	0.6785	1.4163	0.6314	1.5190	5	0.7096	1.4836	0.6600	1.5918
10	0.7642	1.2772	0.7275	1.3423	10	0.7846	1.3101	0.7465	1.3761
15	0.8058	1.2226	0.7730	1.2716	15	0.8175	1.2411	0.7846	1.2913
20	0.8315	1.1915	0.8028	1.2329	20	0.8392	1.2035	0.8119	1.2472

Note: The table presents the simulated critical values to construct the highest density confidence intervals of the AMRE estimators for spot volatility (σ_t) and spot variance (σ_t^2) across various block sizes (k), significance levels ($\alpha \in \{10\%, 5\%\}$), and Stein and quadratic loss functions. For each choice of estimator, k and α, the critical value is numerically computed by a grid search using one million simulations based on Proposition 2. Panel A reports results for spot volatility estimators, while Panel B shows results for spot variance estimators.

Table 2: Asymptotic Properties of AMRE Estimators

Panel A: Estimators for Spot Volatility σ_t

$\hat{\sigma}_{\text{Stein}}(k)$					$\hat{\sigma}_{\text{Quad}}(k)$				
k	Bias	Var	Stein	Quad.	k	Bias	Var	Stein	Quad.
1	-0.0002	0.0622	0.0309	0.0622	1	-0.0586	0.0551	0.0327	0.0585
2	0.0001	0.0307	0.0153	0.0307	2	-0.0296	0.0289	0.0157	0.0298
3	0.0001	0.0203	0.0101	0.0203	3	-0.0197	0.0195	0.0103	0.0198
4	0.0001	0.0151	0.0075	0.0151	4	-0.0148	0.0147	0.0076	0.0149
5	0.0001	0.0120	0.0060	0.0120	5	-0.0118	0.0118	0.0061	0.0119
10	-0.0001	0.0060	0.0030	0.0060	10	-0.0060	0.0059	0.0030	0.0059
15	0.0000	0.0040	0.0020	0.0040	15	-0.0039	0.0039	0.0020	0.0039
20	0.0001	0.0030	0.0015	0.0030	20	-0.0029	0.0030	0.0015	0.0030

Panel B: Estimators for Spot Variance σ_t^2

$\hat{\sigma}^2_{\text{Stein}}(k)$					$\hat{\sigma}^2_{\text{Quad}}(k)$				
k	Bias	Var	Stein	Quad.	k	Bias	Var	Stein	Quad.
1	-0.0003	0.2596	0.1221	0.2596	1	-0.2055	0.1634	0.1471	0.2056
2	0.0002	0.1263	0.0608	0.1263	2	-0.1113	0.0995	0.0676	0.1119
3	0.0003	0.0827	0.0402	0.0827	3	-0.0758	0.0705	0.0433	0.0762
4	0.0001	0.0613	0.0300	0.0613	4	-0.0576	0.0544	0.0318	0.0577
5	0.0001	0.0488	0.0240	0.0488	5	-0.0463	0.0443	0.0251	0.0465
10	-0.0001	0.0240	0.0119	0.0240	10	-0.0236	0.0229	0.0122	0.0234
15	0.0000	0.0159	0.0079	0.0159	15	-0.0157	0.0154	0.0080	0.0157
20	0.0001	0.0119	0.0059	0.0119	20	-0.0117	0.0116	0.0060	0.0118

Note: The table presents asymptotic bias, variance, and risk of AMRE estimators for spot volatility (σ_t) and spot variance (σ_t^2) across various block sizes (k). The results are presented for both Stein and quadratic loss functions. The asymptotic quantities are computed via Monte Carlo integration using one million simulations based on Proposition 2. Panel A reports results for spot volatility estimators, while Panel B shows results for spot variance estimators.

the same optimal estimator minimizes risks for all bowl-shaped loss functions (van der Vaart, 1998), including the two losses considered here. Still, the finding that this occurs for k as low as fifteen is perhaps surprising.

3.2 Risk comparisons with alternative estimators

To more directly highlight the advantages of the AMRE multiple-candlestick estimators, it is instructive to compare the asymptotic risks of the estimators with the risks of some of the alternative suboptimal estimators previously used in the literature.

Our first such comparison speaks directly to the efficiency gains achieved by jointly utilizing the information in k adjacent candlesticks, as opposed to simply combining the corresponding k individual candlestick estimators. Specifically, consider the following ad hoc average estimators:

$$\bar{\sigma}^p_{\text{Stein}}(k) \equiv \frac{1}{k}\sum_{i=1}^{k} \hat{\sigma}^p_{\text{Stein},i}(1), \qquad \bar{\sigma}^p_{\text{Quad}}(k) \equiv \frac{1}{k}\sum_{i=1}^{k} \hat{\sigma}^p_{\text{Quad},i}(1), \tag{3.12}$$

where $\hat{\sigma}^p_{\text{Stein},i}(1)$ and $\hat{\sigma}^p_{\text{Quad},i}(1)$ denote the respective AMRE estimators based solely on the ith candlestick. The estimators defined in (3.12) obviously coincide with the AMRE estimators for $k = 1$. However, they differ from the AMRE estimators based on multiple candlesticks and $k > 1$, by ignoring the interactions among different candlesticks. The calculation of the average estimators in (3.12) also directly mirrors the class of realized volatility estimators studied by Christensen and Podolskij (2007, 2012), Martens and van Dijk (2007), and Li et al. (2025), obtained by replacing the summation of high-frequency squared returns in the traditional realized volatility estimators with the summation of the corresponding high-frequency range-based estimators.

To assess the efficiency loss associated with the imposition of specific functional form and shape restrictions, we also consider the single-candlestick best linear unbiased estimator (BLUE) for the spot volatility proposed by Li et al. (2024), together with the commonly used best quadratic unbiased estimator for spot variance proposed by Garman and Klass (1980):

$$\hat{\sigma}_{\text{BLUE}} \equiv 0.811w - 0.369|r|, \qquad \hat{\sigma}^2_{\text{GK}} \equiv 0.5015w^2 + 0.0095a^2 - 0.3925r^2. \tag{3.13}$$

In parallel to the simple average estimators defined in (3.12), we also analyze the corresponding k-candlestick versions of these shape-restricted estimators obtained by averaging k individual estimators:

$$\bar{\sigma}_{\text{BLUE}}(k) \equiv \frac{1}{k}\sum_{i=1}^{k} \hat{\sigma}_{\text{BLUE},i}, \qquad \bar{\sigma}^2_{\text{GK}}(k) \equiv \frac{1}{k}\sum_{i=1}^{k} \hat{\sigma}^2_{\text{GK},i}, \tag{3.14}$$

where $\hat{\sigma}_{\text{BLUE},i}$ and $\hat{\sigma}^2_{\text{GK},i}$ denote the respective estimators based on the ith candlestick only. Finally, we also consider $\sqrt{\bar{\sigma}^2_{\text{GK}}(k)}$ as an estimator for the spot volatility, and $\big(\bar{\sigma}_{\text{BLUE}}(k)\big)^2$ as an estimator for the spot variance.

All in all, in addition to the AMRE estimators for spot volatility and spot variance under Stein's and quadratic loss for each value of k, this leaves us with four suboptimal estimators for each of the two estimands and loss functions. Table 3 reports the relative efficiency for each of these suboptimal estimators, defined as the ratio of the AMRE estimator's risk to the risk of the suboptimal estimators. Mirroring the format of the previous tables, the results for estimating spot volatility and variance are reported in Panels A and B, respectively, with the left and right portions of the table showing the results for Stein's and quadratic loss, respectively.

Looking at Panel A and the results for spot volatility estimation, it is evident that the $\bar{\sigma}_{\text{Stein}}(k)$ estimator performs quite well under Stein's loss for all values of k. For $k = 1$, it is obviously optimal by design, and as k increases there is only a slight drop in its relative efficiency, which remains above 95% even for $k = 20$. Interestingly, this robustness extends to quadratic loss, even though the $\bar{\sigma}_{\text{Stein}}(k)$ estimator is not specifically tailored to that loss function. The $\bar{\sigma}_{\text{BLUE}}(k)$ estimator also performs quite similar to the $\bar{\sigma}_{\text{Stein}}(k)$ estimator under both loss functions and across all values of k. By comparison, the popular Garman–Klass volatility estimator, and the simple averaged versions thereof, perform noticeably worse, especially for larger values of k. Under both Stein's and quadratic loss, the relative efficiency of $\sqrt{\bar{\sigma}^2_{\text{GK}}(k)}$ is only 90% or lower for $k \geq 5$. Meanwhile, $\bar{\sigma}_{\text{Quad}}(k)$ clearly stands out as the overall worst performing estimator under both loss functions, with rapidly deteriorating relative efficiency for increasing values of k. Even under quadratic loss, where one might naturally expect the estimator to perform reasonably well, its relative efficiency is less than 50% for $k = 20$. This finding again underscores the inadequacy of simply averaging individual estimators, and shrinkage estimators in particular, as this does not achieve any of the bias reduction offered by the AMRE estimator that optimally combines the information in multiple candlesticks.

Turning to panel B and the results for spot variance estimation, the general patterns largely mirror those observed for spot volatility estimation in Panel A. The $\bar{\sigma}^2_{\text{Stein}}(k)$ and $\big(\bar{\sigma}_{\text{BLUE}}(k)\big)^2$ estimators continue to perform relatively well compared to the other suboptimal estimators. Meanwhile, the efficiency of the $\bar{\sigma}^2_{\text{Quad}}(k)$ estimator deteriorates even more rapidly than that of $\bar{\sigma}_{\text{Quad}}(k)$ as k increases, attaining a relative efficiency of less than 25% for $k = 20$ under both loss functions. The efficiency gaps between the AMRE estimators and the suboptimal estimators are also systematically larger for spot variance estimation than for spot volatility estimation, underscoring the importance of choosing the "right" estimator for the relevant loss function.

Table 3: Relative Efficiency of Alternative Estimators

Panel A: Estimators for Spot Volatility σ_t

	Stein's Loss					Quadratic Loss			
k	$\bar{\sigma}_{\text{Stein}}(k)$	$\bar{\sigma}_{\text{Quad}}(k)$	$\bar{\sigma}_{\text{BLUE}}(k)$	$\sqrt{\bar{\sigma}^2_{\text{GK}}(k)}$	k	$\bar{\sigma}_{\text{Stein}}(k)$	$\bar{\sigma}_{\text{Quad}}(k)$	$\bar{\sigma}_{\text{BLUE}}(k)$	$\sqrt{\bar{\sigma}^2_{\text{GK}}(k)}$
1	1.0000	0.9440	0.9908	0.9613	1	0.9408	1.0000	0.9357	0.9593
2	0.9827	0.8819	0.9755	0.9274	2	0.9551	0.9601	0.9503	0.9298
3	0.9743	0.8322	0.9677	0.9131	3	0.9567	0.9116	0.9519	0.9158
4	0.9691	0.7892	0.9627	0.9054	4	0.9564	0.8657	0.9515	0.9080
5	0.9659	0.7517	0.9596	0.9009	5	0.9560	0.8243	0.9510	0.9033
10	0.9580	0.6090	0.9523	0.8896	10	0.9535	0.6637	0.9487	0.8914
15	0.9550	0.5143	0.9493	0.8857	15	0.9521	0.5568	0.9471	0.8868
20	0.9535	0.4454	0.9478	0.8838	20	0.9512	0.4799	0.9462	0.8845

Panel B: Estimators for Spot Variance σ_t^2

	Stein's Loss					Quadratic Loss			
k	$\bar{\sigma}^2_{\text{Stein}}(k)$	$\bar{\sigma}^2_{\text{Quad}}(k)$	$\bar{\sigma}^2_{\text{GK}}(k)$	$\left(\bar{\sigma}_{\text{BLUE}}(k)\right)^2$	k	$\bar{\sigma}^2_{\text{Stein}}(k)$	$\bar{\sigma}^2_{\text{Quad}}(k)$	$\bar{\sigma}^2_{\text{GK}}(k)$	$\left(\bar{\sigma}_{\text{BLUE}}(k)\right)^2$
1	1.0000	0.8301	0.9749	0.9778	1	0.7920	1.0000	0.7650	0.6909
2	0.9634	0.6943	0.9357	0.9703	2	0.8586	0.9018	0.8293	0.8153
3	0.9482	0.6021	0.9191	0.9647	3	0.8794	0.7892	0.8492	0.8601
4	0.9395	0.5329	0.9102	0.9608	4	0.8888	0.6959	0.8585	0.8825
5	0.9344	0.4789	0.9048	0.9582	5	0.8945	0.6213	0.8639	0.8958
10	0.9226	0.3183	0.8918	0.9519	10	0.9037	0.4007	0.8725	0.9218
15	0.9182	0.2392	0.8871	0.9492	15	0.9056	0.2955	0.8741	0.9292
20	0.9160	0.1918	0.8848	0.9477	20	0.9064	0.2342	0.8749	0.9329

Note: The table reports the relative efficiency of each estimator under Stein's and quadratic loss. The relative efficiency is calculated as the ratio of the risk of the AMRE estimator to the risk of the estimator in each column. Panel A reports the results for spot volatility estimation, while Panel B reports the results for spot variance estimation.

In summary, the k-candlestick AMRE estimators often demonstrate sizable efficiency gains compared to some of the suboptimal estimators hitherto used in the literature, especially when considering estimators based on multiple candlesticks. Simply combining individual candlestick estimators in an ad hoc fashion in the construction of k-candlestick estimators, even if the individual estimators are themselves "optimal," is clearly not the "right" thing to do.

3.3 Qualitative features of the optimal estimators

The results in the previous section demonstrated nontrivial efficiency gains for the optimal estimators. At the same time, the complicated functional forms of the estimators make it difficult to discern where the gains are coming from. To help address this question, we directly link the form of the estimators to a set of more intuitive and easily interpretable candlestick features.

The specific features that we use consist of the sample averages and standard deviations of the single-candlestick characteristics $(w_i, |r_i|, a_i)_{1\leq i\leq k}$. That is:

$$\mu_w(k) = \frac{1}{k}\sum_{i=1}^{k} w_i, \qquad \mu_{|r|}(k) = \frac{1}{k}\sum_{i=1}^{k} |r_i|, \qquad \mu_a(k) = \frac{1}{k}\sum_{i=1}^{k} a_i, \tag{3.15}$$

and

$$\begin{aligned} v_w(k) = \sqrt{\frac{1}{k}\sum_{i=1}^{k}\big(w_i - \mu_w(k)\big)^2}, \qquad v_{|r|}(k) = \sqrt{\frac{1}{k}\sum_{i=1}^{k}\big(|r_i| - \mu_{|r|}(k)\big)^2}, \\ v_a(k) = \sqrt{\frac{1}{k}\sum_{i=1}^{k}\big(a_i - \mu_a(k)\big)^2}. \end{aligned} \tag{3.16}$$

We will refer to these six features jointly as $\mathbf{x}(k) \equiv \big(\mu_w(k), \mu_{|r|}(k), \mu_a(k), v_w(k), v_{|r|}(k), v_a(k)\big)$. By directly linking the AMRE estimators to $\mathbf{x}(k)$, we aim to better understand the key "volatility signals" embedded within the candlestick data.[8]

For brevity, we focus our analysis on spot volatility estimation. Specifically, for each AMRE spot volatility estimator, $\hat{\sigma} \in \{\hat{\sigma}_{\text{Stein}}, \hat{\sigma}_{\text{Quad}}\}$, we calculate the following "best subset regression" by running it over a large number of simulations:

$$\min_{\beta\in\mathbb{R}^6} \mathbb{E}\left[\big(\hat{\sigma} - \mathbf{x}(k)\cdot\beta\big)^2\right], \quad \text{s.t. } \|\beta\|_0 \leq q,$$

where $\|\beta\|_0$ counts the number of nonzero coefficients in β, and $q \in \{1, \ldots, 6\}$ is an integer that controls the complexity of the approximation. Hence, by increasing q from 1 to 6, we are able to

[8] These same general types of features are also used more informally by traders and finance practitioners in the context of so-called technical analysis (see, e.g., Nison (2001)).

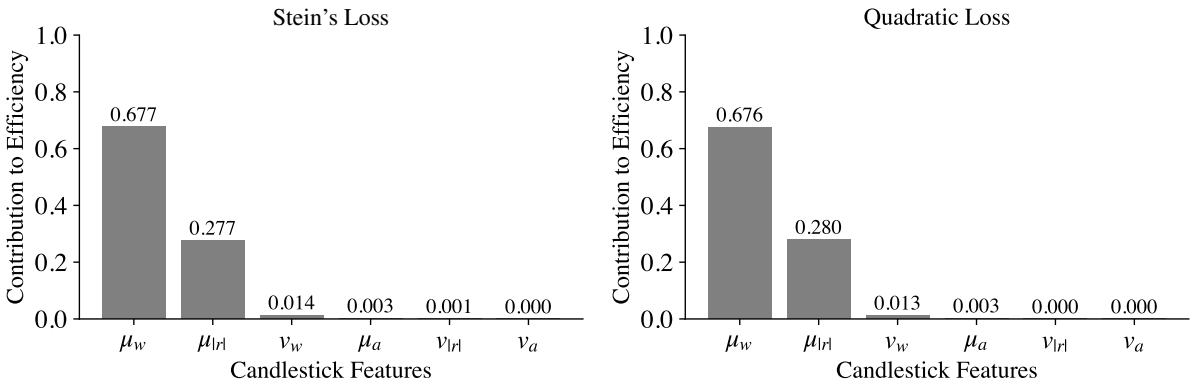

Figure 1: Incremental contribution to relative efficiency by interpretable candlestick features. For each feature, the order of relevance is determined by its selection order in sequential best subset regression, with its contribution measured by the incremental relative efficiency when added to previously selected features.

uncover the most important features for best approximating $\hat{\sigma}$ in descending order, allowing us to rank the features in terms of their relative importance for best approximating a specific AMRE estimator.

Figure 1 shows the resulting incremental relative efficiency gains averaged across $2 \leq k \leq 20$ under both Stein's and quadratic loss. The rankings for both loss functions are the same, in descending order: $\mu_w \succ \mu_{|r|} \succ v_w \succ \mu_a \succ v_{|r|} \succ v_a$. Meanwhile, the two highest ranked features, namely the average range, μ_w, and the average absolute return, $\mu_{|r|}$, obviously account for the vast majority of the variation in the AMRE estimators. Interestingly, w and $|r|$ are also the only building blocks for the simple BLUE estimator studied in Section 3.2. Further along those lines, it readily follows that the average BLUE estimator also studied in Section 3.2 may be expressed as $\bar{\sigma}_{\text{BLUE}}(k) = 0.811\mu_w(k) - 0.369\mu_{|r|}(k)$. The relative ranking of the different features in Figure 1 thus also indirectly helps explain the surprisingly low average relative efficiency loss for the $\bar{\sigma}_{\text{BLUE}}(k)$ estimator previously observed in Panel A in Table 3.

The third most important ranked feature in Figure 1 is v_w, which measures the dispersion among the candlestick ranges. The figure also shows that the incremental contribution of this feature is relatively modest, adding just over 1% on average in terms of the estimators' relative efficiency. The remaining three features, the average asymmetry, μ_a, and the dispersions of the absolute return and the asymmetry, $v_{|r|}$ and v_a, add even less explanatory power.

As representative examples, the approximations based on the top three features for $k = 5$ are:

$$\hat{\sigma}_{\text{Stein}}(5) \approx 0.8238\mu_w - 0.3458\mu_{|r|} - 0.0890v_w, \qquad \hat{\sigma}_{\text{Quad}}(5) \approx 0.8146\mu_w - 0.3468\mu_{|r|} - 0.0809v_w.$$

The projection coefficients for $\mu_{|r|}$ and v_w are both negative, with the latter being relatively small. The negative coefficients indicate that for the same average range, spot volatility tends to be higher when the average absolute return is smaller and when the candlestick ranges are more uniform in size. Table 4 presents the projection coefficients for other values of k, which exhibit the same general pattern.

In summary, estimators that only rely on linear combinations of the six interpretable features in (3.15) and (3.16) are able to achieve an average relative efficiency of 97.2% under both Stein's and quadratic loss. In other words, restricting a candlestick estimator to only depend on these six features invariably results in an efficiency loss of at least 2.8% on average, underscoring the complexity of the AMRE multiple-candlestick estimators and the intricate ways in which they depend on the joint information embedded in all the candlesticks.

4 An Empirical Illustration

Following decades of sustained low inflation, the disruptions stemming from the COVID-19 pandemic resulted in a marked upsurge in U.S. inflation and a renewed interest by macroeconomists in studying inflation and indicators thereof (see, e.g., Bernanke and Blanchard (2025), Ball et al. (2024), and Barro and Bianchi (2025)). Motivated by this increased recent interest, we use the new high-frequency-candlestick-based AMRE spot volatility estimators to analyze the stock market's reaction to the precisely timed releases of the monthly Consumer Price Index (CPI) and the monthly index for Personal Consumption Expenditures (PCE). These are both important indicators of inflationary trends and they also directly influence decisions by the Federal Reserve (Fed). Although the PCE is the official target measure used by the Fed for gauging inflation and determining monetary policy, the CPI announcements often garner more immediate attention. The CPI for a given month is also released before the PCE for that same month, typically by about two weeks. This timing discrepancy means that economists and financial market participants naturally learn and adjust their expectations about the PCE based on the earlier release of the CPI. Correspondingly, asset prices similarly tend to react more sharply to news about CPI than PCE, even though the latter is arguably of more direct importance for the Fed's decision-making process. The importance of the release-schedule in ranking the importance of different news announcements has also previously been emphasized in the literature (see, e.g., the discussion Andersen et al. (2003a)).

Table 4: Best Subset Regression Coefficients for $q = 3$

$\hat{\sigma}_{\text{Stein}}(k)$					$\hat{\sigma}_{\text{Quad}}(k)$				
k	μ_w	$\mu_{\lvert r\rvert}$	v_w	R.Eff.	k	μ_w	$\mu_{\lvert r\rvert}$	v_w	R.Eff.
2	0.8161	-0.3464	-0.0714	0.9862	2	0.7948	-0.3474	-0.0575	0.9871
3	0.8209	-0.3454	-0.0845	0.9806	3	0.8060	-0.3467	-0.0726	0.9816
4	0.8229	-0.3455	-0.0882	0.9764	4	0.8115	-0.3466	-0.0784	0.9774
5	0.8238	-0.3458	-0.0890	0.9731	5	0.8146	-0.3468	-0.0809	0.9741
6	0.8243	-0.3462	-0.0889	0.9706	6	0.8166	-0.3470	-0.0819	0.9715
7	0.8246	-0.3465	-0.0883	0.9687	7	0.8180	-0.3473	-0.0823	0.9696
8	0.8248	-0.3468	-0.0877	0.9671	8	0.8189	-0.3474	-0.0824	0.9680
9	0.8249	-0.3471	-0.0870	0.9659	9	0.8197	-0.3477	-0.0822	0.9667
10	0.8250	-0.3474	-0.0865	0.9649	10	0.8203	-0.3479	-0.0822	0.9657
11	0.8250	-0.3475	-0.0860	0.9640	11	0.8208	-0.3480	-0.0821	0.9647
12	0.8251	-0.3477	-0.0856	0.9633	12	0.8212	-0.3482	-0.0820	0.9640
13	0.8251	-0.3479	-0.0851	0.9626	13	0.8215	-0.3483	-0.0818	0.9633
14	0.8251	-0.3481	-0.0847	0.9620	14	0.8218	-0.3485	-0.0816	0.9627
15	0.8251	-0.3483	-0.0842	0.9616	15	0.8220	-0.3487	-0.0813	0.9622
16	0.8252	-0.3485	-0.0838	0.9612	16	0.8223	-0.3489	-0.0811	0.9618
17	0.8252	-0.3487	-0.0834	0.9608	17	0.8224	-0.3490	-0.0808	0.9614
18	0.8252	-0.3489	-0.0830	0.9604	18	0.8226	-0.3492	-0.0806	0.9610
19	0.8252	-0.3490	-0.0828	0.9601	19	0.8228	-0.3493	-0.0805	0.9606
20	0.8252	-0.3491	-0.0826	0.9598	20	0.8229	-0.3493	-0.0804	0.9603

Note: The table reports the estimated coefficients for the $q = 3$ most important candlestick features for $k = 2, ..., 20$, together with the relative efficiency, calculated as the ratio of the risk of the AMRE estimators to the risk of the approximating estimators.

We focus our analysis on four announcements in the second half of 2023. This was a critical time when the Fed was actively raising interest rates to combat persistent inflation in the wake of the COVID-19 pandemic. During this period, the Federal Open Market Committee (FOMC) also explicitly stated that its monetary policy would be data-dependent, particularly on inflation levels. As such, the releases of the CPI and PCE numbers arguably carried even greater significance than usual, as they directly influenced expectations of future interest rate changes and thus financial asset prices more generally and the stock market in particular. In other words, it is precisely at times like these one might expect the new more accurate estimates to be especially useful.

We rely on high-frequency candlestick data for the E-mini S&P 500 futures at the one-minute frequency.[9] We consider the prices observed one-and-a-half-hour before and after each announcement and estimate the spot volatility over short five-minute-estimation-windows ($k = 5$). A robustness check using other choices of k is provided in the online supplement. It is well documented that scheduled announcements could be accompanied by fixed time price jumps (e.g., Andersen et al. (2003b) and Faust et al. (2007)), volatility jumps (e.g., Bollerslev et al. (2018) and Todorov and Zhang (2025)), drift bursts (e.g., Christensen et al. (2022) and Laurent et al. (2024)), which may cause the Itô semimartingale setting in (2.1) to fail locally at the release time. Therefore, we purposely exclude the one-minute candlestick observed immediately after each release to mitigate the effects of potential violations. To assess the sampling variability of the estimates, we also calculate the 95% HD confidence intervals, following the discussion in Section 3.1. Since the estimation window only spans five minutes, we are able to capture the immediate market reaction before and after each release. For comparison, we also calculate a simple benchmark estimator constructed as the square-root of the sum of the one-minute squared returns over the same five-minute intervals, along with the corresponding confidence intervals.[10] Figure 2 shows the results for the four CPI announcements, with the results for the four PCE announcements depicted in Figure 3. The left columns in both figures show the candlestick-based AMRE estimates, while the right columns display the traditional return-based estimates.

Looking at the candlestick-based AMRE estimates, all of the four news releases for each of the indicators evidently resulted in highly significant changes in the market volatility. Each of the announcements also evidences a fairly similar pattern in the form of an initial sharp rise at the 8:30 a.m. release time, followed by a gradual almost monotone convergence to lower volatility within

[9]The one-minute candlestick data is directly sourced from TickData.com (`https://www.tickdata.com/product/historical-futures-data/`).

[10]This mimics the estimators commonly used in the literature on high-frequency identification via heteroskedasticity; see, e.g., Bollerslev et al. (2018) and the discussion therein. More advanced return-based spot volatility estimators have recently been proposed by Li and Linton (2023) and Figueroa-López and Wu (2024), among others.

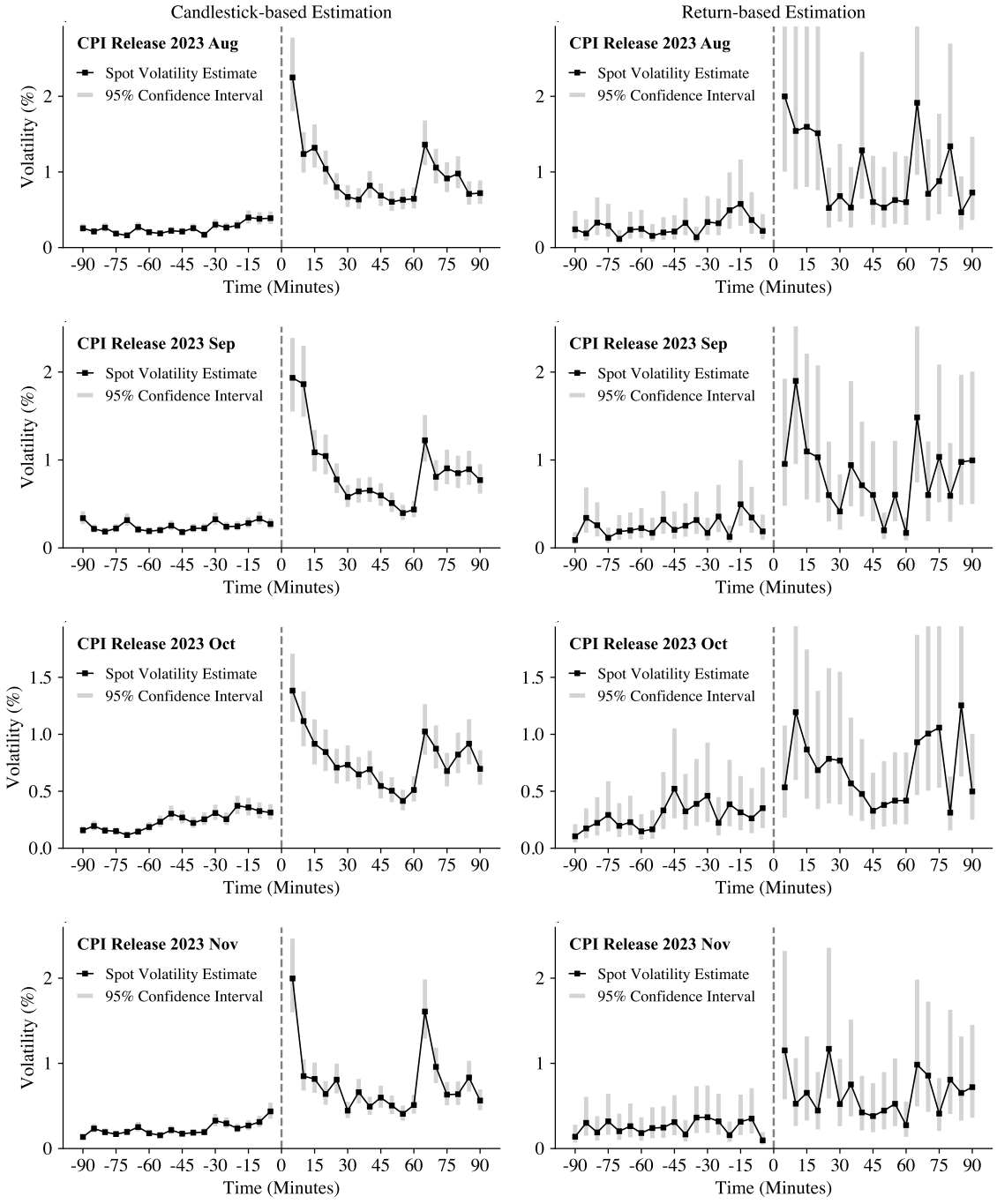

Figure 2: Spot volatility estimation for E-mini S&P 500 futures around CPI releases. Each spot volatility estimator is based on five consecutive candlesticks sampled at a one-minute frequency. The estimation windows are non-overlapping. The left (resp. right) column represents AMRE estimates under Stein's loss (resp. conventional return-based estimates).

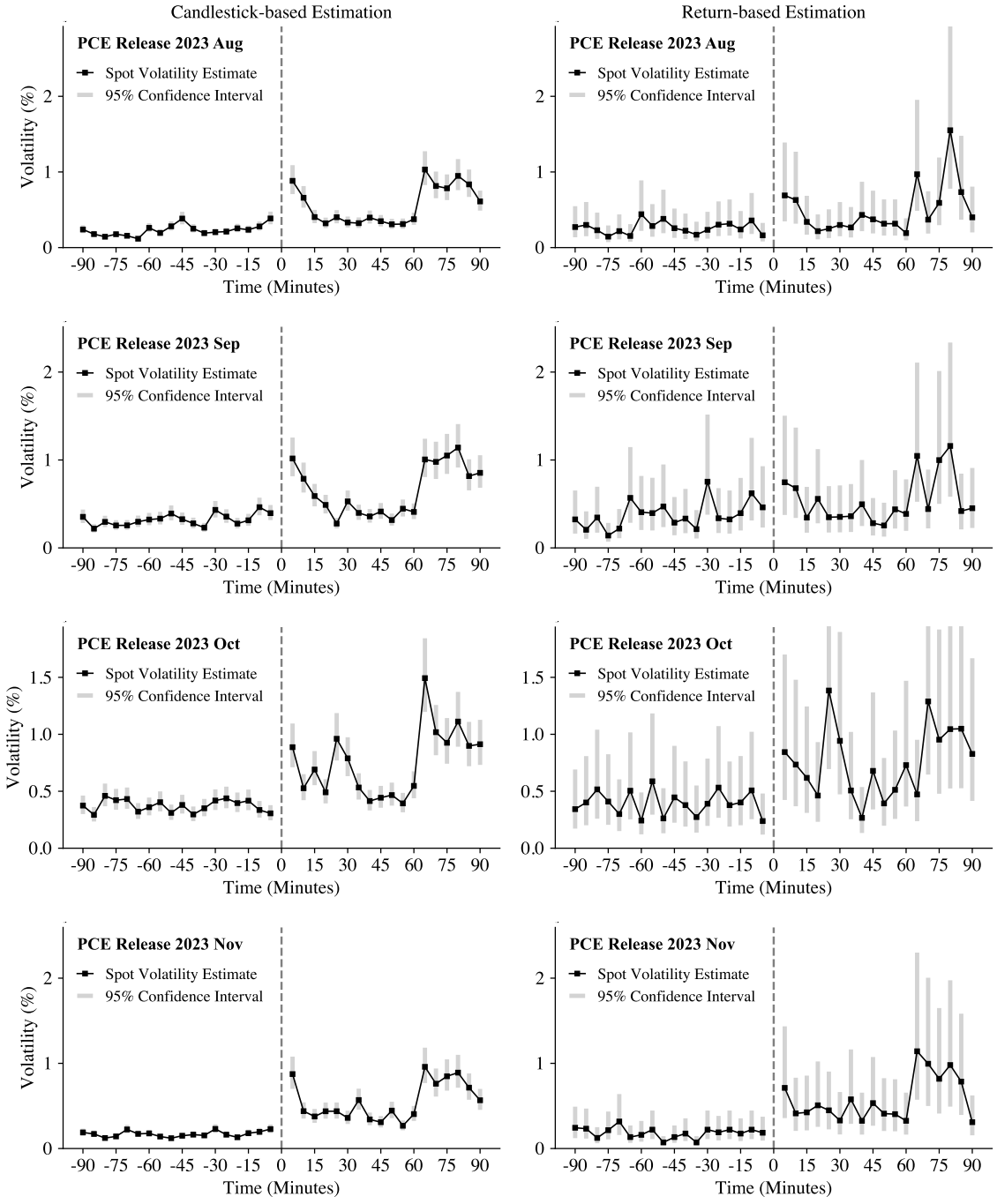

Figure 3: Spot volatility estimation for E-mini S&P 500 futures around PCE releases. Each spot volatility estimator is based on five consecutive candlesticks sampled at a one-minute frequency. The estimation windows are non-overlapping. The left (resp. right) column represents AMRE estimates under Stein's loss (resp. conventional return-based estimates).

the next hour. Then at 9:30 a.m., concurrent with the official opening of the stock exchange, there is another pronounced spike followed by another gradual reversal to more normal levels. This, of course, is also in line with the well-documented U-shaped pattern in volatility generally observed over the trading day. Interestingly, for all four CPI announcements this second opening spike is noticeably lower than the spike observed soon after the announcement, underscoring the economic importance of the CPI. By comparison, the volatility observed at the market opening on the four PCE announcement days often exceed the volatility observed shortly after the news announcement. The overall increases in the volatility associated with the PCE announcements are also significantly less than those for the CPI announcements, again reflecting the importance of the release schedule and the fact that market participants update their expectations about the PCE based on the earlier CPI numbers.

In contrast to these systematic patterns, the traditional return-based volatility estimates shown in the right columns in Figures 2 and 3 appear much more erratic, making it difficult to discern any commonalities in the way in which the market volatility behaves around the news announcements. This, of course, is also directly reflected in the much wider confidence intervals for the return-based estimates. The relatively smooth and consistent patterns observed for the candlestick-based estimates are even more remarkable in light of the fact that there is no "built-in" smoothing across the individual estimates. Instead, the efficient use of the joint information in the five adjacent one-minute candlesticks evidently allows for much more accurate point estimates compared to the traditional return-based estimates, underscoring the usefulness of the estimators as a new practical tool for reliably studying the behavior of volatilities and variances over ultra short time intervals.

5 Concluding Remarks

Leveraging new analytical insights into the structure of optimal spot volatility estimators based on multiple high-frequency candlesticks, we present a novel numerical procedure that enables efficient and accurate numerical computation of the estimators. Our new procedure conveniently bypasses the curse-of-dimensionality problem that has hitherto rendered the implementation of the optimal estimators impractical. We also introduce an exact and easy-to-implement sampling scheme for candlestick data that overcomes the "inward" bias that plagues conventional simulation-based methods for extrema in continuous time settings. Utilizing the new theoretical tools, we numerically compare the asymptotic risks of the estimators that optimally use the information embedded in multiple candlesticks with those of existing estimators. We also provide new insights into the most important features of the candlestick data behind the documented efficiency gains.

We also demonstrate the practical usefulness of the new techniques for estimating and analyzing aggregate stock market volatility around the time of important news announcements pertaining to U.S. inflation.

Our results hold the promise of wider practical usage of the new now computationally feasible optimal candlestick-based estimators, in turn allowing for a better understanding of financial market volatility over short intraday time horizons and the way in which financial markets react to and process new information. Relatedly, the estimators may serve as a valuable new tool in the growing literature predicated on identification through significant high-frequency economic news announcement effects.

Appendix: Proofs

Proof of Proposition 1. We begin by noting that, for each set of candlestick features $(|\tilde{\zeta}_{i,r}|, \tilde{\zeta}_{i,w}, \tilde{\zeta}_{i,a})$, its joint density function $p(|\tilde{\zeta}_{i,r}|, \tilde{\zeta}_{i,w}, \tilde{\zeta}_{i,a})$ is proportional to the $\tilde{g}$ function in (2.9), i.e., $p(|\tilde{\zeta}_{i,r}|, \tilde{\zeta}_{i,w}, \tilde{\zeta}_{i,a}) \propto \tilde{g}(|\tilde{\zeta}_{i,r}|, \tilde{\zeta}_{i,w}, \tilde{\zeta}_{i,a})$. This can be verified from the derivation under (A.8) of Bollerslev et al. (2024). By the independence of Brownian motions across blocks, the joint density of $\tilde{\boldsymbol{\zeta}}_k$ thus satisfies:

$$p(|\tilde{\zeta}_{1,r}|, \tilde{\zeta}_{1,w}, \tilde{\zeta}_{1,a}, \ldots, |\tilde{\zeta}_{k,r}|, \tilde{\zeta}_{k,w}, \tilde{\zeta}_{k,a}) \propto \prod_{i=1}^{k} \tilde{g}(|\tilde{\zeta}_{i,r}|, \tilde{\zeta}_{i,w}, \tilde{\zeta}_{i,a}).$$

We now derive an explicit expression of the conditional expectation $F_{k,q}(\cdot)$ in terms of the above density, which further leads to the desired expressions of the AMRE estimators. By definition of the conditional expectation and the Bayes formula, we have:

$$\begin{aligned} &F_{k,q}\Big(\frac{|r_1|}{w_1}, \frac{a_1}{w_1}, \frac{w_2}{w_1}, \frac{|r_2|}{w_1}, \frac{a_2}{w_1}, \cdots, \frac{w_k}{w_1}, \frac{|r_k|}{w_1}, \frac{a_k}{w_1}\Big) \\ &\quad = \frac{\int_0^\infty w^q \cdot \tilde{p}\big(w, \frac{|r_1|}{w_1}, \frac{a_1}{w_1}, \frac{w_2}{w_1}, \frac{|r_2|}{w_1}, \frac{a_2}{w_1}, \cdots, \frac{w_k}{w_1}, \frac{|r_k|}{w_1}, \frac{a_k}{w_1}\big) dw}{\int_0^\infty \tilde{p}\big(w, \frac{|r_1|}{w_1}, \frac{a_1}{w_1}, \frac{w_2}{w_1}, \frac{|r_2|}{w_1}, \frac{a_2}{w_1}, \cdots, \frac{w_k}{w_1}, \frac{|r_k|}{w_1}, \frac{a_k}{w_1}\big) dw}, \end{aligned} \tag{A.1}$$

where $\tilde{p}$ is the joint density function of $\tilde{\zeta}_{1,w}, \frac{|\tilde{\zeta}_{1,r}|}{\tilde{\zeta}_{1,w}}, \frac{\tilde{\zeta}_{1,a}}{\tilde{\zeta}_{1,w}}, \frac{\tilde{\zeta}_{2,w}}{\tilde{\zeta}_{1,w}}, \frac{|\tilde{\zeta}_{2,r}|}{\tilde{\zeta}_{1,w}}, \frac{\tilde{\zeta}_{2,a}}{\tilde{\zeta}_{1,w}}, \cdots, \frac{\tilde{\zeta}_{k,w}}{\tilde{\zeta}_{1,w}}, \frac{|\tilde{\zeta}_{k,r}|}{\tilde{\zeta}_{1,w}}, \frac{\tilde{\zeta}_{k,a}}{\tilde{\zeta}_{1,w}}$, which can be expressed in terms of the density of $\tilde{\boldsymbol{\zeta}}_k$ since the Jacobian of this transformation is w^{3k-1}:

$$\begin{aligned} &\tilde{p}\bigg(w, \frac{|\tilde{\zeta}_{1,r}|}{\tilde{\zeta}_{1,w}}, \frac{\tilde{\zeta}_{1,a}}{\tilde{\zeta}_{1,w}}, \frac{\tilde{\zeta}_{2,w}}{\tilde{\zeta}_{1,w}}, \frac{|\tilde{\zeta}_{2,r}|}{\tilde{\zeta}_{1,w}}, \frac{\tilde{\zeta}_{2,a}}{\tilde{\zeta}_{1,w}}, \cdots, \frac{\tilde{\zeta}_{k,w}}{\tilde{\zeta}_{1,w}}, \frac{|\tilde{\zeta}_{k,r}|}{\tilde{\zeta}_{1,w}}, \frac{\tilde{\zeta}_{k,a}}{\tilde{\zeta}_{1,w}}\bigg) \\ &\quad = w^{3k-1} p\bigg(w\frac{|\tilde{\zeta}_{1,r}|}{\tilde{\zeta}_{1,w}}, w, w\frac{\tilde{\zeta}_{1,a}}{\tilde{\zeta}_{1,w}}, w\frac{|\tilde{\zeta}_{2,r}|}{\tilde{\zeta}_{1,w}}, w\frac{\tilde{\zeta}_{2,w}}{\tilde{\zeta}_{1,w}}, w\frac{\tilde{\zeta}_{2,a}}{\tilde{\zeta}_{1,w}}, \cdots, w\frac{|\tilde{\zeta}_{k,r}|}{\tilde{\zeta}_{1,w}}, w\frac{\tilde{\zeta}_{k,w}}{\tilde{\zeta}_{1,w}}, w\frac{\tilde{\zeta}_{k,a}}{\tilde{\zeta}_{1,w}}\bigg) \\ &\quad \propto w^{3k-1} \prod_{i=1}^{k} \tilde{g}\bigg(w\frac{|\tilde{\zeta}_{i,r}|}{\tilde{\zeta}_{1,w}}, w\frac{\tilde{\zeta}_{i,w}}{\tilde{\zeta}_{1,w}}, w\frac{\tilde{\zeta}_{i,a}}{\tilde{\zeta}_{1,w}}\bigg). \end{aligned}$$

Consider the integral below for some $m \in \{0, q\}$ and by a change of variable $v \equiv w/\tilde{\zeta}_{1,w}$, we have:

$$\int_0^\infty w^{m+3k-1} \prod_{i=1}^k \tilde{g}\Big(w\frac{|\tilde{\zeta}_{i,r}|}{\tilde{\zeta}_{1,w}}, w\frac{\tilde{\zeta}_{i,w}}{\tilde{\zeta}_{1,w}}, w\frac{\tilde{\zeta}_{i,a}}{\tilde{\zeta}_{1,w}}\Big)dw = \tilde{\zeta}_{1,w}^{m+3k} \int_0^\infty v^{m+3k-1} \prod_{i=1}^k \tilde{g}(v|\tilde{\zeta}_{i,r}|, v\tilde{\zeta}_{i,w}, v\tilde{\zeta}_{i,a})dv.$$

Setting $\tilde{\boldsymbol{\zeta}}_k = \mathbf{C}_k$ and applying the above result to the numerator and denominator of the right-hand side of (A.1), and notice that the proportionality constants cancel out by division, we arrive at:

$$\begin{aligned} &F_{k,q}\Big(\frac{|r_1|}{w_1}, \frac{a_1}{w_1}, \frac{w_2}{w_1}, \frac{|r_2|}{w_1}, \frac{a_2}{w_1}, \cdots, \frac{w_k}{w_1}, \frac{|r_k|}{w_1}, \frac{a_k}{w_1}\Big) \\ &= w_1^q \cdot \frac{\int_0^\infty v^{q+3k-1} \prod_{i=1}^k \tilde{g}(v|r_i|, vw_i, va_i)dv}{\int_0^\infty v^{3k-1} \prod_{i=1}^k \tilde{g}(v|r_i|, vw_i, va_i)dv} = w_1^q \cdot \frac{M_{k,q}(\mathbf{C}_k)}{M_{k,0}(\mathbf{C}_k)}. \end{aligned}$$

The desired expressions of $\hat{\sigma}^p_{\text{Stein}}(k)$ and $\hat{\sigma}^p_{\text{Quad}}(k)$ follow immediately from the above expression and (2.6). Finally, we note that a sufficient condition for $M_{k,p}(\mathbf{C}_k)$ to exist is $3k + p - 1 \geq 0$, since the integrand $\tilde{g}$ is finite at $v = 0$ and decays to zero exponentially fast as $v \to \infty$. Therefore, $k \geq (1-2p)/3 \vee 1$ ensures that both $M_{k,p}(\mathbf{C}_k)$ and $M_{k,2p}(\mathbf{C}_k)$ exist, so that $\hat{\sigma}^p_{\text{Stein}}(k)$ and $\hat{\sigma}^p_{\text{Quad}}(k)$ are well-defined. *Q.E.D.*

Proof of Proposition 2. To prove $(r, h, l) \stackrel{d}{=} (\tilde{\zeta}_r, \tilde{\zeta}_h, \tilde{\zeta}_l)$, it suffices to show that:

$$r \stackrel{d}{=} \tilde{\zeta}_r, \quad h|r \stackrel{d}{=} \tilde{\zeta}_h|\tilde{\zeta}_r, \quad l|h, r \stackrel{d}{=} \tilde{\zeta}_l|\tilde{\zeta}_r, \tilde{\zeta}_h. \tag{A.2}$$

The first relation is obvious. For the second relation, we start with the joint law of $(\tilde{\zeta}_h, \tilde{\zeta}_r)$ which can be found in, e.g., Shepp (1979):

$$f_{\tilde{\zeta}_h, \tilde{\zeta}_r}(h, r) = \frac{2(2h-r)}{\sqrt{2\pi}} \exp\Big\{\Big(-\frac{(2h-r)^2}{2}\Big)\Big\} = -2\phi'(2h-r),$$

where $h \geq (r \vee 0)$. The density of $\tilde{\zeta}_h$ conditional on $\tilde{\zeta}_r$ is thus

$$f_{\tilde{\zeta}_h|\tilde{\zeta}_r}(h|r) = \frac{-\phi'(2h-r)}{\phi(r)} = 2(2h-r)\exp\{-2h(h-r)\}.$$

Direct integration reveals that

$$F_{\tilde{\zeta}_h|\tilde{\zeta}_r}(h|r) = \int_{r\vee 0}^h f_{\tilde{\zeta}_h|\tilde{\zeta}_r}(s|r)ds = 1 - \exp\{2(r-h)h\},$$

from which one can directly calculate its inverse function

$$F^{-1}_{\tilde{\zeta}_h|\tilde{\zeta}_r}(u|r) = \frac{1}{2}\big(r + \sqrt{r^2 - 2\log(1-u)}\big).$$

By the probability integral transform, the second relation in Equation (A.2) is then immediate. For the last relation, we derive the density of $\tilde{\zeta}_l$ conditioning on $\tilde{\zeta}_r$ and $\tilde{\zeta}_h$:

$$\begin{aligned} f_{\tilde{\zeta}_l|\tilde{\zeta}_r,\tilde{\zeta}_h}(l|r,h) &= \frac{f_{\tilde{\zeta}_r,\tilde{\zeta}_h,\tilde{\zeta}_h}(r,h,l)}{f_{\tilde{\zeta}_h,\tilde{\zeta}_r}(h,r)} \\ &= -2\sum_{m=-\infty}^{\infty}\left(m^2\frac{\phi''\big(r-2m(h-l)\big)}{\phi'(2h-r)} - m(m+1)\frac{\phi''\big(r-2mh+2(m-1)l\big)}{\phi'(2h-r)}\right), \end{aligned}$$

where $l \leq r \wedge 0$ and the analytical form of $f_{\tilde{\zeta}_r,\tilde{\zeta}_h,\tilde{\zeta}_h}(r,h,l)$ can be found in, e.g., Feller (1951). It is now straightforward to verify that $F'(l;r,h) = f_{\tilde{\zeta}_l|\tilde{\zeta}_r,\tilde{\zeta}_h}(l|r,h)$, and one can also check that $F(-\infty;r,h) = 0$ and $F(r\wedge 0;r,h) = 1$. In other words, $F(l;r,h)$ is the cumulative distribution function of $\tilde{\zeta}_l$ conditional on $\tilde{\zeta}_r$ and $\tilde{\zeta}_h$. The solution $v = F(l;r,h)$ is thus an implicit probability integral transform, and the third relation in Equation (A.2) readily follows, which completes the proof. *Q.E.D.*

References

Andersen, T. G. and T. Bollerslev (1998): "Answering the Skeptics: Yes, Standard Volatility Models do Provide Accurate Forecasts," *International Economic Review*, 39, 885–905.

——— (2018): *Volatility*, Edward Elgar Publishing.

Andersen, T. G., T. Bollerslev, P. F. Christoffersen, and F. X. Diebold (2006): "Volatility and Correlation Forecasting," in *Handbook of Economic Forecasting*, Elsevier, vol. 1, 777–878.

Andersen, T. G., T. Bollerslev, F. X. Diebold, and C. Vega (2003a): "Micro Effects of Macro Announcements: Real-Time Price Discovery in Foreign Exchange," *American Economic Review*, 93, 38–62.

——— (2003b): "Micro effects of macro announcements: Real-time price discovery in foreign exchange," *American economic review*, 93, 38–62.

Asmussen, S., P. Glynn, and J. Pitman (1995): "Discretization error in simulation of one-dimensional reflecting Brownian motion," *The Annals of Applied Probability*, 5, 875–896.

Ball, L. M., D. Leigh, and P. Mishra (2024): "Understanding U.S. Inflation During the Covid Era," NBER Working Paper.

Barndorff-Nielsen, O. E. and N. Shephard (2002): "Econometric Analysis of Realized Volatility and Its Use in Estimating Stochastic Volatility Models," *Journal of the Royal Statistical Society. Series B.*, 64, 253–280.

Barro, R. J. and F. Bianchi (2025): "Fiscal influences on inflation in OECD countries, 2020–2023," *The Economic Journal*, forthcoming.

Bernanke, B. and O. Blanchard (2025): "What Caused the U.S. Pandemic-Era Inflation?" *American Economic Journal: Macroeconomics*, 17, 1–35.

Bibinger, M., J. M. Jirak, and M. Reiss (2016): "Volatility estimation under one-sided errors with applications to limit order books," *Annals of Applied Probability*, 26, 2754–2790.

Bladt, M., S. Finch, and M. Sørensen (2016): "Simulation of Multivariate Diffusion Bridges," *Journal of the Royal Statistical Society, Series B*, 78, 343–369.

Bladt, M. and M. Sørensen (2014): "Simple Simulation of Diffusion Bridges with Application to Likelihood Inference for Diffusions," *Bernoulli*, 20, 645–675.

Bollerslev, T., R. F. Engle, and D. B. Nelson (1994): "ARCH Models," in *Handbook of Econometrics*, Elsevier, 2959–3038.

Bollerslev, T., J. Li, and Q. Li (2024): "Optimal Nonparametric Range-Based Volatility Estimation," *Journal of Econometrics*, 238, 105548.

Bollerslev, T., J. Li, and Z. Liao (2021): " Fixed-k Inference for Volatility," *Quantitative Economics*, 12, 1053–1084.

Bollerslev, T., J. Li, and Y. Xue (2018): "Volume, volatility, and public news announcements," *Review of Economic Studies*, 4, 116–136.

Brown, L. (1968): "Inadmissibility of the Usual Estimators of Scale Parameters in Problems with Unknown Location and Scale Parameters," *Annals of Mathematical Statistics*, 39, 29–48.

Christensen, K., R. Oomen, and R. Renò (2022): "The drift burst hypothesis," *Journal of Econometrics*, 227, 461–497.

Christensen, K. and M. Podolskij (2007): "Realized Range-Based Estimation of Integrated Variance," *Journal of Econometrics*, 141, 323–349.

——— (2012): "Asymptotic Theory of Range-Based Multipower Variation," *Journal of Financial Econometrics*, 10, 417–456.

Faust, J., J. H. Rogers, S.-Y. B. Wang, and J. H. Wright (2007): "The high-frequency response of exchange rates and interest rates to macroeconomic announcements," *Journal of Monetary Economics*, 54, 1051–1068.

Feller, W. (1951): "The Asymptotic Distribution of the Range of Sums of Independent Random Variables," *Annals of Mathematical Statistics*, 22, 427–432.

Figueroa-López, J. E. and B. Wu (2024): "Kernel estimation of spot volatility with microstructure noise using pre-averaging," *Econometric Theory*, 40, 558–607.

Foster, D. P. and D. B. Nelson (1996): "Continuous Record Asymptotics for Rolling Sample Variance Estimators," *Econometrica*, 64, 139–174.

Garman, M. B. and M. J. Klass (1980): "On the Estimation of Security Price Volatilities from Historical Data," *The Journal of Business*, 53, 67–78.

Ghysels, E., A. C. Harvey, and E. Renault (1996): "Stochastic Volatility," in *Handbook of Statistics*, Elsevier, vol. 14, 119–191.

Ghysels, E., P. Mykland, and E. Renault (2023): "In-Sample Asymptotics and Cross-Sample Efficiency Gains for High Frequency Data Statistics," *Econometric Theory*, 39, 70–106.

Laurent, S., R. Renò, and S. Shi (2024): "Realized drift," *Journal of Econometrics*, 105813.

Li, J., D. Wang, and Q. Zhang (2024): "Reading the Candlesticks: An OK Estimator for Volatility," *Review of Economics and Statistics*, 106, 1114–1128.

Li, Y., I. Nolte, S. Nolte, and S. Yu (2025): "Realized candlestick wicks," *Journal of Econometrics*, 250, 106014.

Li, Z. M. and O. Linton (2023): "Robust estimation of integrated and spot volatility," *Journal of Econometrics*, 105614.

Martens, M. and D. van Dijk (2007): "Measuring Volatility with the Realized Range," *Journal of Econometrics*, 138, 181–207.

Nison, S. (2001): *Japanese Candlestick Charting Techniques*, Prentice Hall Press, 2nd ed.

Parkinson, M. (1980): "The Extreme Value Method for Estimating the Variance of the Rate of Return," *The Journal of Business*, 53, 61–65.

Shepp, L. A. (1979): "The Joint Density of the Maximum and Its Location for a Wiener Process with Drift," *Journal of Applied Probability*, 16, 423–427.

Stoer, J. and R. Bulirsch (2002): "Introduction to Numerical Analysis," *Texts in Applied Mathematics*.

Todorov, V. (2019): "Nonparametric Spot Volatility from Options," *Annals of Applied Probability*, 29, 3590–3636.

Todorov, V. and Y. Zhang (2022): "Information Gains from Using Short-Dated Options for Measuring and Forecasting Volatility," *Journal of Applied Econometrics*, 37, 368–391.

——— (2025): "Testing for anticipated changes in spot volatility at event times," *Econometric Theory*, 41, 1–34.

van der Vaart, A. W. (1998): *Asymptotic Statistics*, Cambridge Series in Statistical and Probabilistic Mathematics, Cambridge University Press.